LETTER

Flows of X–ray gas reveal the disruption of a star by a massive black hole

Jon M. Miller[1], Jelle S. Kaastra[2,3,4], M. Coleman Miller[5], Mark T. Reynolds[1], Gregory Brown[6], S. Bradley Cenko[7,8], Jeremy J. Drake[9], Suvi Gezari[5], James Guillochon[10], Kayhan Gultekin[1], Jimmy Irwin[11], Andrew Levan[6], Dipankar Maitra[12], W. Peter Maksym[11], Richard Mushotzky[5], Paul O'Brien[13], Frits Paerels[14], Jelle de Plaa[2], Enrico Ramirez-Ruiz[15], Tod Strohmayer[7] & Nial Tanvir[13]

Tidal forces close to massive black holes can violently disrupt stars that make a close approach. These extreme events are discovered via bright X-ray[1–4] and optical/ultraviolet[5,6] flares in galactic centres. Prior studies based on modelling decaying flux trends have been able to estimate broad properties, such as the mass accretion rate[6,7]. Here we report the detection of flows of hot, ionized gas in high-resolution X-ray spectra of a nearby tidal disruption event, ASASSN-14li in the galaxy PGC 043234. Variability within the absorption-dominated spectra indicates that the gas is relatively close to the black hole. Narrow linewidths indicate that the gas does not stretch over a large range of radii, giving a low volume filling factor. Modest outflow speeds of a few hundred kilometres per second are observed; these are below the escape speed from the radius set by variability. The gas flow is consistent with a rotating wind from the inner, super-Eddington region of a nascent accretion disk, or with a filament of disrupted stellar gas near to the apocentre of an elliptical orbit. Flows of this sort are predicted by fundamental analytical theory[8] and more recent numerical simulations[7,9–14].

ASASSN-14li was discovered in images obtained on 22 November 2014 (modified Julian day MJD 56,983), at a visual magnitude of $V = 16.5$ (ref. 15) by the All-Sky Automated Survey for Supernovae (ASASSN). Follow-up observations found this transient source to coincide with the centre of the galaxy PGC 043234 (originally Zwicky VIII 211), to within 0.04 arcseconds (ref. 15). This galaxy lies at a redshift of $z = 0.0206$, or a luminosity distance of 90.3 Mpc (for $H_0 = 73$ km s^{-1}, $\Omega_{matter} = 0.27$, $\Omega_\Lambda = 0.73$), making ASASSN-14li the closest disruption event discovered in over ten years. The discovery magnitudes indicated a substantial flux increase over prior, archival optical images of this galaxy. Follow-up observations with the Swift space observatory's X-ray Telescope[16,17] (XRT) established a new X-ray source at this location[15].

Archival X-ray studies rule out the possibility that PGC 043234 harbours a standard active galactic nucleus that could produce bright flaring. PGC 043234 is not detected in the ROSAT All-Sky Survey[18]. Using the online interface to the data, the background count rate for sources detected in the vicinity is 0.002 counts s^{-1} arcmin^{-2}. With standard assumptions (see Methods), this rate corresponds to a luminosity of $L \approx 4.8 \times 10^{40}$ erg s^{-1}, which is orders of magnitude below a standard active nucleus.

Theory predicts that early tidal disruption event (TDE) evolution should be dominated by a bright, super-Eddington accretion phase, and be followed by a characteristic $t^{-5/3}$ decline as disrupted material

interacts and accretes[8,19]. Detections of winds integral to super-Eddington accretion have not been reported previously, but $t^{-5/3}$ flux decay trends in the ultraviolet part of the spectrum (where disk emission from active nuclei typically peaks) are now a standard signature of TDEs in the literature[5,6]. Figure 1 shows the flux decay of ASASSN-14li, as observed by Swift. A fit to the UVM2-filter data assuming an index of $\alpha = -5/3$ gives a disruption date of $t_0 \approx 56,948 \pm 3$ (MJD). The V-band light is consistent with a shallower $t^{-5/12}$ decay; this can indicate direct thermal emission from the disk, or reprocessed emission[7,11] (see Methods).

We triggered approved XMM-Newton programs to study ASASSN-14li soon after its discovery. Although the space observatory XMM-Newton carries several instruments, the spectra from the two Reflection Grating Spectrometer (RGS) units are the focus of this analysis. We were also granted a Director's Discretionary Time
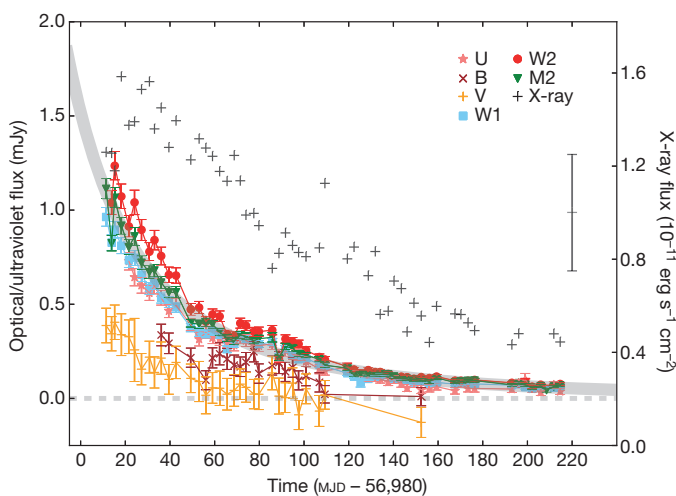
Figure 1 | The multi-wavelength light curves of ASASSN-14li clearly signal a tidal disruption event. The light curves are based on monitoring observations with the Swift satellite. The errors shown on plotting symbols are the 1σ confidence limits on the flux in each band (V, B, U, UVW1 (here W1), UVM2 (M2), UVW2 (W2). Contributions from the host galaxy have been subtracted (see Methods). The UVM2 filter samples the ultraviolet light especially well. The grey shading depicts the $t^{-5/3}$ flux decay predicted by fundamental theory[8,19]. The X-ray flux points carry relatively large errors; a representative error bar is shown at right. Fits to the decay curve are described in the main text and in the Methods.

[1]Department of Astronomy, The University of Michigan, 1085 South University Avenue, Ann Arbor, Michigan 48103, USA. [2]SRON Netherlands Institute for Space Research, Sorbonnelaan 2, 3584 CA Utrecht, The Netherlands. [3]Department of Physics and Astronomy, Universiteit Utrecht, PO Box 80000, 3508 TA Utrecht, The Netherlands. [4]Leiden Observatory, Leiden University, PO Box 9513, 2300 RA Leiden, The Netherlands. [5]Department of Astronomy, The University of Maryland, College Park, Maryland 20742, USA. [6]Department of Physics, University of Warwick, Coventry CV4 7AL, UK. [7]Joint Space-Science Institute, University of Maryland, College Park, Maryland 20742, USA. [8]Astrophysics Science Division, NASA Goddard Space Flight Center, MC 661, Greenbelt, Maryland 20771, USA. [9]Smithsonian Astrophysical Observatory, 60 Garden Street, Cambridge, Massachusetts 02138, USA. [10]The Institute for Theory and Computation, Harvard–Smithsonian Center for Astrophysics, 60 Garden Street, Cambridge, Massachusetts 02138, USA. [11]Department of Physics and Astronomy, University of Alabama, PO Box 870324, Tuscaloosa, Alabama 35487, USA. [12]Department of Physics and Astronomy, Wheaton College, Norton, Massachusetts 02766, USA. [13]Department of Physics and Astronomy, University of Leicester, University Road, Leicester LE1 7RH, UK. [14]Columbia Astrophysics Laboratory and Department of Astronomy, Columbia University, 550 West 120th Street, New York, New York 10027, USA. [15]Department of Astronomy and Astrophysics, University of California, Santa Cruz, California 95064, USA.

Table 1 | Modelling of the high-resolution X-ray spectra reveals ionized flows of gas

Mission	XMM-Newton	XMM-Newton	XMM-Newton	XMM-Newton	Chandra	XMM-Newton
Observation ID	0694651201	0722480201	0722480201	0722480201	17566, 17567	0694651401
Comment	Monitoring	Long stare	Stare (low)	Stare (high)	None	Monitoring
Start (MJD)	56,997.98	56,999.54	56,999.94	57,000.0	56,999.97, 57,002.98	57,023.52
Duration (ks)	22	94	36	58	35, 45	23.6
$F_{X,b}$ (10^{-11} erg cm^{-2} s^{-1})	2.7 ± 0.7	3.2 ± 0.4	3.4 ± 0.3	3.4 ± 0.2	$2.5^{+0.2}_{-0.3}$	2.68 ± 0.08
$L_{X,b}$ (10^{44} erg s^{-1})	2.9 ± 0.7	2.2 ± 0.3	2.2 ± 0.2	2.0 ± 0.1	$1.7^{+0.1}_{-0.2}$	3.2 ± 0.1
$F_{X,f}$ (10^{-11} erg cm^{-2} s^{-1})	1.2 ± 0.3	1.2 ± 0.2	1.07 ± 0.08	1.24 ± 0.08	$1.0^{+0.1}_{-0.2}$	1.19 ± 0.04
$L_{X,f}$ (10^{44} erg s^{-1})	0.25 ± 0.06	0.21 ± 0.03	0.19 ± 0.01	0.21 ± 0.01	$0.17^{+0.01}_{-0.02}$	0.27 ± 0.01
$N_{H,MW}$ (10^{20} cm^{-2})	2.6*	2.6 ± 0.6	2.6*	2.6*	2.6*	2.6*
$N_{H,HG}$ (10^{20} cm^{-2})	1.4*	1.4 ± 0.5	1.4*	1.4*	1.4*	1.4*
$N_{H,TDE}$ (10^{22} cm^{-2})	0.7 ± 0.2	$1.3^{+0.9}_{-0.4}$	$0.1^{+0.3}_{-0.2}$	$0.9^{+0.2}_{-0.3}$	$0.5^{+0.4}_{-0.1}$	0.5 ± 0.1
$\log \xi$ (erg cm s^{-1})	3.6 ± 0.1	4.1 ± 0.2	4.1 ± 0.1	$3.9^{+0.3}_{-0.1}$	$3.9^{+0.1}_{-0.2}$	3.7 ± 0.1
v_{rms} (km s^{-1})	130 ± 30	110^{+30}_{-20}	60^{+60}_{-50}	120 ± 20	120^{+40}_{-30}	230^{+60}_{-50}
v_{shift} (km s^{-1})	-180 ± 60	-210 ± 40	-360 ± 50	-130^{-50}_{+70}	-500^{+60}_{-70}	-490 ± 70
kT (eV)	50.0 ± 0.09	51.4 ± 0.1	50.0 ± 0.4	52.6 ± 0.4	52.6 ± 0.3	49.7 ± 0.9
Emitting area (10^{25} cm^2)	5.7 ± 1.4	3.7 ± 0.5	4.0 ± 0.3	3.0 ± 0.2	$2.5^{+0.1}_{-0.2}$	6.1 ± 0.2
χ^2/ν	704.8/567	870.5/563	687.8/564	726.8/565	266.5/178	626.5/566

Each spectrum was fitted with a simple blackbody continuum, modified by photoionized absorption via the *pion* model, and interstellar absorption in the host galaxy PGC 043234 and the Milky Way. The fits were made using SPEX[28], minimizing a χ^2 statistic. In all cases, 1σ errors are quoted. Where a parameter is quoted with an asterisk, the listed parameter was not varied. X-ray fluxes F_X and luminosities L_X listed with the subscript 'b' for 'broad' were extrapolated from the fitting band to the 1.24–124 Å band; those with the subscript 'f' represent values for the 18–35 Å fitting band. Interstellar column densities N_H are separately measured for the Milky Way ($N_{H,MW}$) at zero redshift and the host galaxy PGC 043234 ($N_{H,HG}$) at a redshift of $z = 0.0206$. These parameters were measured in the XMM-Newton 'long stare' and then fixed in fits to other spectra. Variable parameters in the photoionization model are listed together; the negative v_{shift} values indicate a blueshift relative to the host galaxy. Here ξ is the ionization parameter of the gas, v_{rms} is the root-mean-square velocity width of the spectral lines, k is Boltzmann's constant, T is temperature and ν is the number of degrees of freedom.

observation with the Chandra X-ray Observatory, using its Low Energy Transmission Grating spectrometer (LETG), paired with its High Resolution Camera for spectroscopy (HRC-S).

The 18–35 Å X-ray spectra of ASASSN-14li are clearly thermal in origin, so we modelled the continuum with a single blackbody, modified by interstellar absorption in PGC 043234 and the Milky Way, and absorption from blueshifted, ionized gas local to the TDE. The self-consistent photoionization code *pion*[20] was used to model the complex absorption spectra (see Table 1 and Methods).

Assuming that the highest bolometric luminosity derived from fits to the high-resolution spectra ($L = 3.2 \pm 0.1 \times 10^{44}$ erg s^{-1}) corresponds to the Eddington limit, a black-hole mass of $2.5 \times 10^6 M_\odot$,

where $M_\odot$ is the mass of the Sun, is inferred. The blackbody emission measured from fits to the time-averaged XMM-Newton spectrum gives an emitting area of 3.7×10^{25} cm^2, implying $r = 1.7 \times 10^{12}$ cm for a spherical geometry.

This is consistent with the innermost stable circular orbit around a black hole of mass $M \approx 1.9 \times 10^6 M_\odot$. Modelling of the Swift light curves (see Fig. 1), using a self-consistent treatment of direct and reprocessed light from an elliptical accretion disk[7] gives a mass in the range of $M \approx (0.4–1.2) \times 10^6 M_\odot$ (see Methods). Together, the thermal spectrum, implied radii and the run of emission from X-rays to optical bands unambiguously signal the presence of an accretion disk in ASASSN-14li.
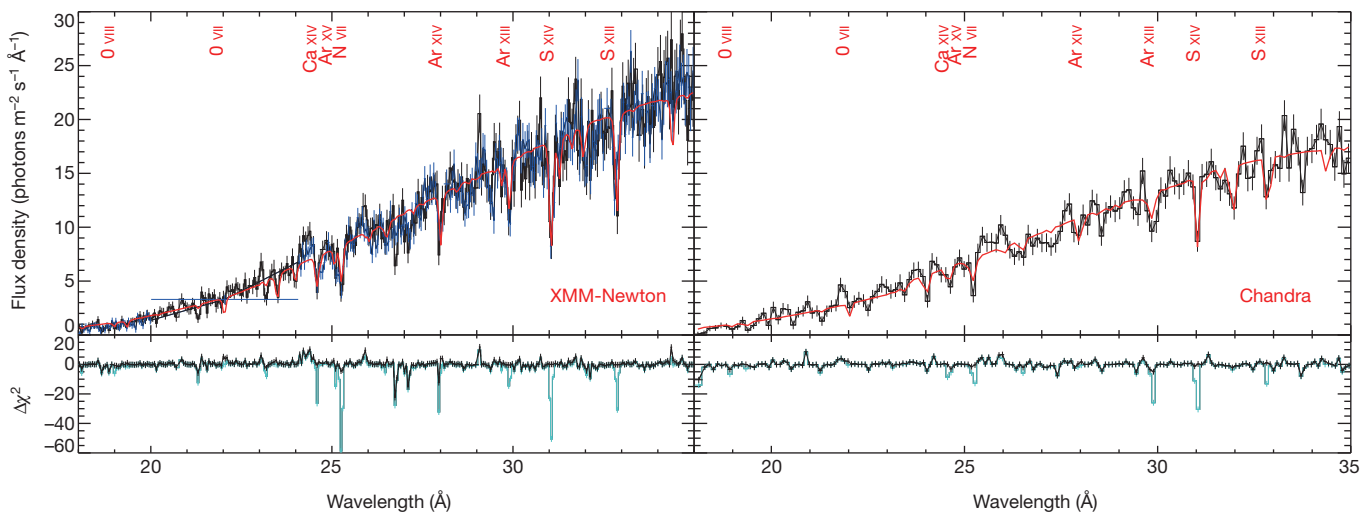
Figure 2 | The high-resolution X-ray spectra of ASASSN-14li reveal blueshifted absorption lines. Spectra from the 'long stare' with XMM-Newton and the combined Chandra spectrum are shown. XMM-Newton spectra from the RGS1 and RGS2 units are shown in black and blue, respectively; the RGS2 unit is missing a detector in the 20–24 Å band. The best-fit photoionized absorption model for the outflowing gas detected in each spectrum is shown in red (see Methods), and selected strong lines are indicated. Below each spectrum, the goodness-of-fit statistic ($\Delta\chi^2$) is shown before (cyan) and after (black) modelling the absorbing gas. The errors on the spectra are 1σ confidence limits on the flux in each bin.
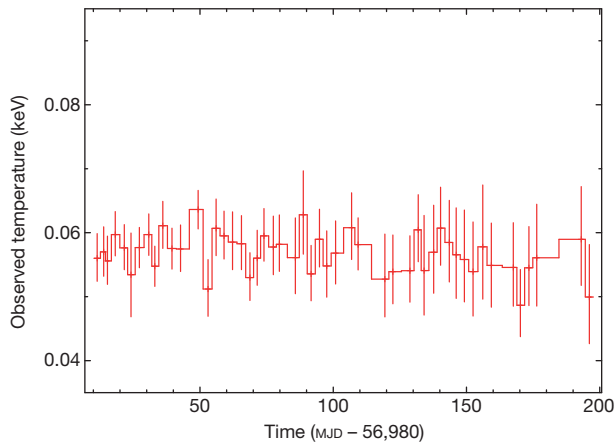
Figure 3 | The temperature of the blackbody continuum emission from ASASSN-14li is steady over time. The temperature measured in simple blackbody fits to Swift/XRT monitoring observations is plotted versus time. Errors are 1σ confidence intervals. The temperature is remarkably steady, contrasting strongly with the declining fluxes shown in Fig. 1. Recent theory suggests that winds may serve to maintain steady temperatures in some TDEs[14].

Figure 2 shows the best-fit model for the spectra obtained in the 'long stare' with the XMM-Newton/RGS (see Table 1 and Methods). An F-test finds that photoionized X-ray absorption is required in fits to these spectra at more than the 27σ level of confidence, relative to a spectral model with no such absorption. The model captures the majority of the strong absorption lines, giving $\chi^2 = 870.5$ for 563 degrees of freedom (see Table 1). The strongest lines in the spectrum coincide with ionized charge states of N, O, S, Ar and Ca. Only solar abundances are required to describe the spectra. The Chandra spectrum independently confirms these results in broad terms, and requires absorption at more than the 6σ level of confidence.

A hard lower limit on the radius of the absorbing gas is set by the blackbody continuum. The best radius estimate probably comes from variability timescales within the XMM-Newton 'long stare'. Analysis of specific time segments within the 'long stare', as well as flux-selected segments, reveals that the absorption varies (see Table 1 and Methods). This sets a relevant limit of $r \lesssim c\delta t$, or $r \lesssim 3 \times 10^{15}$ cm, where r is the radius of the absorbing gas relative to the central engine, c is the speed of light, and δt is the time interval of the variability. Although the column density and ionization do not vary significantly, the blueshift of the gas does. During the initial third of the observation, the blueshift is larger, $v_{shift} = -360 \pm 50$ km s^{-1}, but falls to $v_{shift} = -130^{-50}_{+70}$ km s^{-1} in the final two-thirds. Shorter monitoring observations with XMM-Newton reveal evolution of the absorbing gas, including changes in ionization and column density, before and after the 'long stare' (see Table 1 and Methods).

Fundamental theoretical treatments of TDEs predict an initial near-Eddington or super-Eddington phase[8]; this is confirmed in more recent theoretical studies[9,12,21]. The high-resolution X-ray spectra were obtained within the predicted time frame for super-Eddington accretion, for our estimates of the black-hole mass[22]. Although the ionization parameter of the observed gas is high, the ionizing photon distribution peaks at a low energy, and the wind could be driven by radiation force. Such flows are naturally clumpy, and may be similar to the photospheres of novae[23]. Given the strong evidence of an accretion disk in our observations of ASASSN-14li, the X-ray outflow is best associated with a wind from the inner regions of a nascent, super-Eddington accretion disk. The local escape speed at an absorption radius of $r \approx 10^4\ GM/c^2$ (appropriate for $M \approx 10^6 M_\odot$; G is Newton's gravitational constant) exceeds the observed outflow line-of-sight speed of the gas, but Keplerian rotation is not encoded in absorption, and projection effects are also important. The small width of the absorption lines relative to the escape velocity may also indicate a low volume filling factor, consistent with a clumpy outflow or shell.

The existing observations show a general trend towards higher outflow speeds with time. Corresponding changes in ionization and column density are more modest, and not clearly linked to outflow speed[24]. However, some recent work has predicted higher outflow speeds in an initial super-Eddington disk regime, and lower outflow speeds in a subsequent thin disk regime[9,12]. An observation in an earlier, more highly super-Eddington phase might have observed broader lines and higher outflow speeds; future observations of new TDEs can test this.

Figure 3 shows the time evolution of the blackbody temperature measured in Swift/XRT monitoring observations. The temperature is remarkably constant, especially in contrast to the optical/ultraviolet decline shown in Fig. 1. Observations of steady blackbody temperatures, despite decaying multi-wavelength light curves in some TDEs[6,25], have recently been explained through winds[14]. Evidence of winds in our data supports this picture.

The low gas velocities may also be consistent with disrupted stellar gas on an elliptical orbit in a nascent disk, near the apocentre. This picture naturally gives a low filling factor, resulting in a small total mass in absorbing gas (see Methods). Recent numerical simulations predict that a fraction of the disrupted material in a TDE will circularize slowly[13], and that flows will be filamentary[26], while stellar gas that is more tightly bound can form an inner, Eddington-limited or super-Eddington disk more quickly.

The highly ionized, blueshifted gas discovered in our high-resolution X-ray spectra of ASASSN-14li confirms both fundamental and very recent theoretical predictions for the structure and evolution of TDEs. By pairing high-resolution X-ray spectroscopy with an ever-increasing number of TDE detections, it will become possible to test models of accretion disk formation and evolution, and to explore strong-field gravitation around massive black holes[27].

Online Content Methods, along with any additional Extended Data display items and Source Data, are available in the online version of the paper; references unique to these sections appear only in the online paper.

1. Bade, N., Komossa, S. & Dahlem, M. Detection of an extremely soft X-ray outburst in the HII-like nucleus of NGC 5905. *Astron. Astrophys.* **309**, L35–L38 (1996).
2. Komossa, S. & Greiner, J. Discovery of a giant and luminous X-ray outburst from the optically inactive galaxy pair RX J1242.6–1119. *Astron. Astrophys.* **349**, L45–L48 (1999).
3. Esquej, P. et al. Candidate tidal disruption events from the XMM-Newton slew survey. *Astron. Astrophys.* **462**, L49–L52 (2007).
4. Cappelluti, N. et al. A candidate tidal disruption event in the Galaxy cluster Abell 3571. *Astron. Astrophys.* **495**, L9–L12 (2009).
5. Gezari, S. et al. UV/optical detections of candidate tidal disruption events by GALEX and CFHTLS. *Astrophys. J.* **676**, 944–969 (2008).
6. Gezari, S. et al. An ultraviolet-optical flare from the tidal disruption of a helium-rich stellar core. *Nature* **485**, 217–220 (2012).
7. Guillochon, J., Manukian, H. & Ramirez-Ruiz, E. PS1–10jh: the disruption of a main-sequence star of near-solar composition. *Astrophys. J.* **783**, 23 (2014).
8. Rees, M. J. Tidal disruption of stars by black holes of 10^6–10^8 solar masses in nearby galaxies. *Nature* **333**, 523–528 (1988).
9. Strubbe, L. E. & Quataert, E. Optical flares from the tidal disruption of stars by massive black holes. *Mon. Not. R. Astron. Soc.* **400**, 2070–2084 (2009).
10. Lodato, G., King, A. R. & Pringle, J. E. Stellar disruption by a supermassive black hole: is the light curve really proportional to $t^{-5/3}$? *Mon. Not. R. Astron. Soc.* **392**, 332–340 (2009).
11. Lodato, G. & Rossi, E. M. Multiband light curves of tidal disruption events. *Mon. Not. R. Astron. Soc.* **410**, 359–367 (2011).
12. Strubbe, L. E. & Quataert, E. Spectroscopic signatures of the tidal disruption of stars by massive black holes. *Mon. Not. R. Astron. Soc.* **415**, 168–180 (2011).
13. Shiokawa, H., Krolik, J. H., Cheng, R. M., Piran, T. & Noble, S. C. General relativistic hydrodynamic simulation of accretion flow from a stellar tidal disruption. *Astrophys. J.* **804**, 85 (2015).
14. Miller, M. C. Disk winds as an explanation for slowly evolving temperatures in tidal disruption events. *Astrophys. J.* **805**, 83 (2015).
15. Jose, J. et al. ASAS-SN discovery of an unusual nuclear transient in PGC 043234. *Astron. Telegr.* **6777**, 1 (2014).
16. Gehrels, N. et al. The Swift Gamma-Ray Burst Mission. *Astrophys. J.* **611**, 1005–1020 (2004).
17. Burrows, D. N. et al. The Swift X-ray telescope. *Space Sci. Rev.* **120**, 165–195 (2005).

18. Voges, W. *et al.* The ROSAT All-Sky Survey bright source catalogue. *Astron. Astrophys.* **349,** 389–405 (1999).
19. Phinney, E. S. in *The Center of the Galaxy* (ed. Morris, M.) *IAU Symp.*, **136,** 543–553 (Kluwer Academic, 1989).
20. Kaastra, J. S., Mewe, R. & Nieuwenhuijzen, H. in *UV and X-ray Spectroscopy of Astrophysical and Laboratory Plasmas* (eds Yamashita, K. & Watanabe, T.) 411–414 (Universal Academy Press, Tokyo, 1996).
21. Loeb, A. & Ulmer, A. Optical appearance of the debris of a star disrupted by a massive black hole. *Astrophys. J.* **489,** 573–578 (1997).
22. Piran, T., Svirski, G., Krolik, J., Cheng, R. M. & Shiokawa, H. Disk formation versus disk accretion—what powers tidal disruption events? *Astrophys. J.* **806,** 164 (2015).
23. Shaviv, N. J. The theory of steady-state super-Eddington winds and its application to novae. *Mon. Not. R. Astron. Soc.* **326,** 126–146 (2001).
24. Ramírez, J. M. Kinematics from spectral lines for AGN outflows based on time-independent radiation-driven wind theory. *Rev. Mex. Astron. Astrofis.* **47,** 385–399 (2011).
25. Holoien, T. W.-S. *et al.* ASASSN-14ae: a tidal disruption event at 200 Mpc. *Mon. Not. R. Astron. Soc.* **445,** 3263–3277 (2014).
26. Guillochon, J. & Ramirez-Ruiz, E. A dark year for tidal disruption events. *Astrophys. J.* **809,** 166 (2015).
27. Stone, N. & Loeb, A. Observing Lense-Thirring precession in tidal disruption flares. *Phys. Rev. Lett.* **108,** 061302 (2012).
28. Kaastra, J. S., Mewe, R. & Raassen, T. New results on X-ray models and atomic data. *Highlights Astron.* **13,** 648–650 (2005).

Author Contributions J.M.M. led the Chandra and XMM-Newton data reduction and analysis, with contributions from J.S.K., J.J.D. and J.d.P. M.T.R. led the Swift data reduction and analysis (with help from S.B.C., S.G. and R.M.). M.C.M., E.R.-R. and J.G. provided theoretical insights. G.B., K.G., J.I., A.L., D.M., W.P.M., P.O'B., F.P., T.S. and N.T. contributed to the discussion and interpretation.

Author Information Reprints and permissions information is available at www.nature.com/reprints. The authors declare no competing financial interests. Readers are welcome to comment on the online version of the paper. Correspondence and requests for materials should be addressed to J.M.M. (jonmm@umich.edu).

METHODS

Estimates of prior black-hole luminosity. Using the ROSAT All-Sky Survey[18], the region around the host galaxy, PGC 043234, was searched for point sources. No sources were found. Points in the vicinity of the host galaxy were examined to derive a background count rate of 0.002 counts s^{-1}. Assuming the Milky Way column density $N_{H,MW}$ along this line of sight, and taking a typical Seyfert X-ray spectral index of $\Gamma = 1.7$, this count rate translates into $L \approx 4.8 \times 10^{40}$ erg s^{-1}. This limit is orders of magnitude below a Seyfert or quasar luminosity.

Optical/ultraviolet monitoring observations and data reduction. Swift[16] monitors transient and variable sources via co-aligned X-ray (XRT, 0.3–10 keV) and ultraviolet–optical (UVOT, 170–650 nm) telescopes. High-cadence monitoring of ASASSN-14li with UVOT has continued in six bands: V, B, U, UVW1, UVM2, and UVW2 (central wavelength $\lambda_c = 550$ nm, 440 nm, 350 nm, 260 nm, 220 nm and 190 nm).

All observations were processed using the latest HEASOFT (http://heasarc.gsfc.nasa.gov/docs/software/lheasoft/) suite and calibrations. Individual optical/ultraviolet exposures were astrometrically corrected and sub-exposures in each filter were summed. Source fluxes were then extracted from an aperture of 3″ radius, and background fluxes were extracted from a source-free region to the east of ASASSN-14li owing to the presence of a (blue) star lying 10 arcsec to the South, using UVOTMAGHIST, a routine within HEASOFT.

To estimate the host contamination, we have measured the host flux in 3″ aperture (matched to the aperture used for the UVOT photometry) in pre-outburst Sloan Digital Sky Survey (SDSS[29]), 2 Micron All-Sky Survey (2MASS[30]), and GALEX[31] images. We took extra care to deblend the GALEX data, where the large point spread function (PSF) resulted in contamination from the star about 10″ to the South. We estimated the uncertainty in each host flux by varying the inclusion aperture from 2″ to 4″.

We then fitted the host photometry to synthetic galaxy templates using the Fitting and Assessment of Synthetic Templates (FAST[32]) code. We employed stellar templates from the[33] catalogue, and allowed the star-formation history, extinction law, and initial mass function to vary over the full range of parameters allowed by the software. All best-fit models had stellar masses of about $10^{9.2} M_\odot$, low ongoing star-formation rates (at most about $10^{-1.5} M_\odot$ yr^{-1}), and modest line-of-sight extinction ($A_V \lesssim 0.4$ mag).

We integrated the resulting galaxy template spectra over each UVOT filter bandpass to estimate the host count rate. For the uncertainty in this value, we adopt either the root-mean-square spread of the resulting galaxy template models, or 10% of the inferred count rate, whichever value was larger. We then subtracted these values from our measured (coincidence-loss corrected) photometry of the host plus transient, to isolate the component that is due to TDE. For reference, our inferred count rates for each UVOT filter are 5.7 ± 0.6 s^{-1} for V, 9.4 ± 0.9 s^{-1} for B, 4.0 ± 0.4 s^{-1} for U, 0.83 ± 0.08 s^{-1} for UVW1, 0.29 ± 0.03 s^{-1} for UVM2, and 0.49 ± 0.05 s^{-1} for UVW2. Figure 1 shows the host-subtracted optical and ultraviolet light curves ASASSN-14li.

Fits to the UVOT/UVM2 light curve. The UVM2 filter provides the most robust trace of the mass accretion rate in a TDE like ASASSN-14li; it has negligible transmission at optical wavelengths[34,35]. Fits to the UVM2 light curve with a power law of the form $f(t) = f_0 \times (t + t_0)^\alpha$ with a fixed index of $\alpha = -5/3$ imply a disruption date of $t_0 = 56,980 \pm 3$ (MJD). This model achieves a fair characterization of the data; high fluxes between days 80 and 100 (in the units of Fig. 1) result in a poor statistical fit ($\chi^2/\nu = 1.7$, where $\nu = 54$ degrees of freedom). If the light curve is fitted with a variable index, a value of -2.6 ± 0.3 is measured (90% confidence). This model achieves an improved fit ($\chi^2/\nu = 1.4$, for $\nu = 53$ degrees of freedom), but it does not tightly constrain the disruption date, placing t_0 in the MJD 56,855–56,920 range. That disruption window is adjacent to an interval wherein the ASASSN monitoring did not detect the source[15], making it less plausible than the fit at $\alpha = -5/3$.

The optical bands appear to have a shallower decay curve than the ultraviolet bands. Recent theory[11] predicts that optical light produced via thermal disk emission should show a decay consistent with $t^{-5/12}$; this might also be due to reprocessing[7]. The V-band data are consistent with this prediction, though the data are of modest quality and a broad range of decays are permitted.

X-ray monitoring observations and data reduction. The Swift XRT[17] is a charge-coupled device. In such cameras, photon pile-up occurs when two or more photons land within a single detection box during a single frame time. This causes flux distortions and spectral distortions to bright sources. Such distortions are effectively avoided by extracting events from an annular region, rather than from a circle at the centre of the telescope PSF. We therefore extracted source spectra from annuli with an inner radius of 12 arcsec (5 pixels), and an outer radius of 50 arcsec. Background flux was measured in an annular region extending from 140 arcsec to 210 arcsec.

Standard redistribution matrices were used; an ancillary response file was created with the *xrtmkarf* tool (a routine within HEASOFT) using a vignetting corrected exposure map. The source spectra were rebinned to have 20 counts per bin with *grppha*. In all spectral fits, we adopted a lower spectral bound of 0.3 keV (36 Å). The upper bound on spectral fits varied depending on the boundary of the last bin with at least 20 counts; this was generally around 1 keV (12 Å).

The XRT spectra were fitted with a model consisting of absorption in the Milky Way of a blackbody emitted at the redshift of the TDE, that is, *pha(zashift(bbodyrad))*, where $N_H \equiv 4 \times 10^{20}$ cm^{-2} and $z \equiv 0.0206$. The evolution of the best-fit temperature of this blackbody component is displayed in Fig. 3.

The blackbody temperature values measured from the Swift XRT are slightly higher ($kT \approx 7$–10 eV) than those measured with XMM-Newton and Chandra. If an outflow component with fiducial parameters is included in the spectral model anyway, the XRT temperatures are then in complete agreement with those measured using XMM-Newton and Chandra.

Estimates of the black-hole mass. Luminosity values inferred for the band over which the high-resolution spectra are actually fitted, and for a broader band, are listed in Table 1. Taking the broader values as a proxy for a true bolometric fit, the highest implied soft X-ray luminosity is measured in the last XMM-Newton monitoring observation, giving $L \approx 3.2 \times 10^{44}$ erg s^{-1}. The Eddington luminosity for standard hydrogen-rich accretion is $L_{Edd} = 1.3 \times 10^{38}$ erg s^{-1} $(M/M_\odot)$. This implies a black-hole mass of $M \approx 2.5 \times 10^6 M_\odot$.

Blackbody continua imply size scales, and, if we assume that optically thick blackbody emission can only originate at radii larger than the innermost stable circular orbit (ISCO), also masses. For a non-spinning Schwarzschild black hole, $r_{ISCO} = 6GM/c^2$. The blackbody emission measured in fits to the time-averaged XMM-Newton 'long stare' gives an emitting area of 3.7×10^{25} cm^2; implying $r = 1.7 \times 10^{12}$ cm for a spherical geometry. The actual geometry may be more disk-like, but the inner flow may be a thick disk that is better represented by a spherical geometry. If the black hole powering ASASSN-14li is not spinning, this size implies a black-hole mass of $M \approx 1.9 \times 10^6 M_\odot$.

We also estimated the mass of the black hole at the heart of ASASSN-14li by fitting the host-subtracted light curves (see Fig. 1) using the Monte Carlo software TDEFit[7]. This software assumes that emission is produced within an elliptical accretion disk where the mass accretion rate follows the fallback rate[36] onto the black hole with a viscous delay[26]. This emission is then partly reprocessed into the ultraviolet/optical part of the spectrum by an optically thick layer[21]. Super-Eddington accretion is treated by presuming that a fitted fraction of the Eddington excess is converted into light that is reprocessed by the same optically thick layer. This excess can be produced either with an unbound wind[9,37], or with the energy deposited by shocks in the circularization process[13,22].

The software performs a maximum-likelihood analysis to determine the combinations of parameters that reproduce the observed light curves. We utilize the ASASSN, UVOT and XRT data in our light-curve fitting; the most likely models produce good fits to all bands simultaneously. Within the context of this TDE model, a black-hole mass of $(0.4$–$1.2) \times 10^6 M_\odot$ (1σ) is derived.

Spectroscopic observations, data reduction and analysis. Table 1 lists the observation identification number, start time, and duration of all of the XMM-Newton and Chandra observations considered in our work.

The XMM-Newton data were reduced using the standard Science Analysis System (SAS version 13.5.0) tools and the latest calibration files. The *rgsproc* routine was used to generate spectral files from the source, background spectral files, and instrument response files. The spectra from the RGS1 and RGS2 units were fitted jointly. Prior to fitting models, all XMM-Newton spectra were binned by a factor of five for clarity and sensitivity.

The Chandra data were reduced using the standard Chandra Interactive Analysis of Observations (CIAO version 4.7) suite, and the latest associated calibration files. Instrument response files were constructed using the *fullgarf* and *mkgrmf* routines. The first-order spectra from each observation were combined using the tool *add grating orders*, and spectra from each observation were then added using *add grating spectra*.

The spectra were analysed using the SPEX suite version 2.06 (ref. 20). The fitting procedure minimized a χ^2 statistic. The spectra are most sensitive in the 18–35 Å band, and all fits were restricted to this range. Within SPEX, absorption from the interstellar medium in the Milky Way was modelled using the model 'hot'; a separate 'hot' component was included to allow for interstellar medium (ISM) absorption within PGC 043234 at its known redshift (using the *reds* component in SPEX). The photoionized outflow was modelled using the *pion* component within the SPEX suite.

pion[20] includes numerous lines from intermediate charge states that are lacking in similar astrophysics packages. The fits explored in this analysis varied the gas column density ($N_{H,TDE}$), the gas ionization parameter (ξ, where $\xi = L/nr^2$, and L is luminosity, n is the hydrogen number density and r is the distance between the

ionizing source and absorbing gas), the root-mean-square velocity of the gas (v_{rms}), and the bulk shift of the gas relative to the source, in the source frame (v_{shift}). Spectra from segments within the 'long stare' made with XMM-Newton were made by using the SAS tool *tabgtigen* to create *good time interval* files to isolate periods within the light curves of the RGS data.

The Chandra/LETG spectra were dispersed onto the HRC, which has a relatively high instrumental background. Fitting the spectra only in the 18–35 Å band served to limit the contributions of the background. Nevertheless, the Chandra spectra are less sensitive than the best XMM-Newton spectra of ASASSN-14li (see Fig. 2). Prior to fitting, spectra from the two exposures were added and then binned by a factor of three.

Figure 2 includes plots of the $\Delta\chi^2$ goodness-of-fit statistic as a function of wavelength, before and after including *pion* to model the ionized absorption. There is weak evidence of emission lines in the spectra, perhaps with a P Cygni profile (see below). The best-fit models for the high-resolution spectra predict one absorption line at 34.5 Å (H-like C VI) that is not observed; small variations to abundances could resolve this disparity.

Blueshifts as small as $200\,km\,s^{-1}$ are measured in the XMM-Newton/RGS using the *pion* model. According to the XMM-Newton User's Handbook, available through the mission website, http://xmm.esac.esa.int/external/xmm_user_support/documentation/index.shtml, the absolute accuracy of the first-order wavelength scale is 6 mÅ. At 18 Å this corresponds to a velocity of $100\,km\,s^{-1}$; at 35 Å, this corresponds to a velocity of $51\,km\,s^{-1}$. The model predicts numerous lines across the 18–35 Å band that are clearly detected; especially with this leverage, the small shifts we have measured with XMM-Newton are robust. In particular, the difference in blueshift between the low- and high-flux phases of the 'long stare', $-360\pm50\,km\,s^{-1}$ versus $-130^{+70}_{-50}\,km\,s^{-1}$, is greater than the absolute calibration uncertainties. Differences observed in the outflow velocities between XMM-Newton observations are as large, or larger, and also robust.

The lower sensitivity of the Chandra spectra is evident in the relatively poor constraints achieved on the column density of the ionized X-ray outflow $N_{H,TDE}$ (see Table 1). Similarly, the relatively high outflow velocity measured in the Chandra spectra should be viewed with a degree of caution. The outflow velocity changes from about $500\,km\,s^{-1}$ to just $-130\pm130\,km\,s^{-1}$, for instance, when the binning factor is increased from three to five. We have found no reports in the literature of a systematic wavelength offset between contemporary high-resolution spectra obtained with XMM-Newton and Chandra.

The small number of high-resolution spectra complicates efforts to discern trends. The velocity width of the absorbing gas is fairly constant over time, but there is a general trend towards higher blue-shifts. There is no clear trend in column density or ionization parameter with time.

Diffuse gas mass, outflow rates and filling factors. There is no a priori constraint on the density of the absorbing gas. Taking the maximum radius implied by variability within XMM-Newton 'long stare', $r\lesssim3\times10^{15}\,cm$, and manipulating the ionization parameter equation ($\xi = Ln^{-1}r^{-2}$, where L is the luminosity, n is the number density and r is the absorbing radius), we can derive an estimate of the density: $n\approx2\times10^9\,cm^{-3}$. Even assuming a uniformly filled sphere out to a radius of $r=3\times10^{15}\,cm$, a total mass of $M\approx4\times10^{32}\,g$ is implied, or approximately $0.2M_\odot$.

The true gas mass within r is likely to be orders of magnitude lower, owing to clumping and a very low volume filling factor. Using the measured value of $N_{H,TDE}$ and assuming $n\approx2\times10^9\,cm^{-3}$, $N_{H,TDE}=n\Delta r$ gives a value of $\Delta r\approx6.5\times10^{12}\,cm$. The filling factor can be estimated using $\Delta r/r\approx0.002$. The total mass enclosed out to a distance r is then reduced accordingly, down to $4\times10^{-4}M_\odot$, assuming a uniform density within r. This is a small value, plausible either for a clumpy wind or gas within a filament executing an elliptical orbit.

Formally, the mass outflow rate in ASASSN-14li can be adapted from the case where the density is known, and written as:

$$\dot{M}_{out} = \mu m_p \Omega Lv C_v \xi^{-1}$$

where μ is the mean atomic weight ($\mu = 1.23$ is typical), m_p is the mass of the proton, Ω is the covering factor ($0\leq\Omega\leq4\pi$), L is the ionizing luminosity, v is the outflow velocity, C_v is the line-of-sight global (volume) filling factor and ξ is the ionization parameter. Using the values obtained in fits to the XMM-Newton 'long stare' (see Table 1), for instance, $\dot{M}_{out}\approx7.9\times10^{23}\Omega C_v\,g\,s^{-1}$. Taking the value of C_v derived above, an outflow rate of $\dot{M}_{out}\approx1.5\times10^{21}\Omega\,g\,s^{-1}$ results. The kinetic power in the outflow is given by $L_{kin}=0.5\dot{M}v^2$; using the same values assumed to estimate the mass outflow rate, $L_{kin}\approx3.3\times10^{35}\,erg\,s^{-1}$.

Emission from the diffuse outflow. We synthesized a plausible wind emission spectrum by coupling the *pion* and *hyd* models within SPEX. The *hyd* code enables spectra to be constructed based on the output of hydrodynamical simulations. As inputs, the *hyd* code requires the electron temperature and ion concentrations for a gas; these were taken from our fits with *pion*. We included the resulting emission component in experimental fits to the XMM-Newton 'long stare'. The best-fit model gives an emission measure of $(1.0\pm0.3)\times10^{64}\,cm^{-3}$, a redshift (relative to the host) of $270^{+350}_{-150}\,km\,s^{-1}$, and an ionization parameter of $\log\xi = 4.3\pm0.1$.

According to an F-test, the emission component is only required at the 3σ level; however, it has some compelling properties. Combined with the blueshifted absorption spectrum, the redshifted emission gives P Cygni profiles. For the gas density of $n\approx2\times10^9\,cm^{-3}$ derived previously, the emission measure gives a radius of about $10^{15}\,cm$, comparable to the size scale inferred from absorption variability.

The strongest lines predicted by the emission model include He-like O VII, and H-like charge states of C, N and O. This model does not account for other emission line-like features in the spectra, which are more likely to be artefacts from spectral binning, or calibration or modelling errors. Emission features in the O K-edge region may be real, but caution is warranted. Other features are more easily discounted given that they differ between the RGS1 and RGS2 spectra.

Code availability. All of the data reduction and spectroscopic fitting routines and packages used in this work are publicly available. The light-curve modelling package, TDEFit[7], is proprietary at this time owing to ongoing code development; a public release is planned within the coming year.

29. Ahn, C. P. *et al.* The Tenth Data Release of the Sloan Digital Sky Survey: first spectroscopic data from the SDSS-III Apache Point Observatory Galactic Evolution Experiment. *Astrophys. J. Suppl. Ser.* **211**, 17 (2014).
30. Skrutskie, M. F. *et al.* The Two Micron All Sky Survey (2MASS). *Astron. J.* **131**, 1163–1183 (2006).
31. Martin, D. C. *et al.* The Galaxy Evolution Explorer: a space ultraviolet survey mission. *Astrophys. J.* **619**, L1–L6 (2005).
32. Kriek, M. *et al.* An ultra-deep near-infrared spectrum of a compact quiescent galaxy at z = 2.2. *Astrophys. J.* **700**, 221–231 (2009).
33. Bruzual, G. & Charlot, S. Stellar population synthesis at the resolution of 2003. *Mon. Not. R. Astron. Soc.* **344**, 1000–1028 (2003).
34. Poole, T. S. *et al.* Photometric calibration of the Swift ultraviolet/optical telescope. *Mon. Not. R. Astron. Soc.* **383**, 627–645 (2008).
35. Breeveld, A. A. *et al.* An updated ultraviolet calibration for the Swift/UVOT. *AIP Conf. Ser.* (eds McEnery, J. E., Racusin, J. L. & Gehrels, N.), **1358**, 373–376 (American Institute of Physics, 2011).
36. Guillochon, J. & Ramirez-Ruiz, E. Hydrodynamical simulations to determine the feeding rate of black holes by the tidal disruption of stars: the importance of the impact parameter and stellar structure. *Astrophys. J.* **767**, 25 (2013).
37. Vinkó, J. *et al.* A luminous, fast rising UV-transient discovered by ROTSE: a tidal disruption event? *Astrophys. J.* **798**, 12 (2015).